



HAL
open science

Reprocessing of artificial UV-weathered wood flour reinforced polypropylene composites

L. Soccalingame, Perrin Didier, J.-C. Bénézet, S. Mani, F. Coiffier, E. Richaud, Anne Bergeret

► **To cite this version:**

L. Soccalingame, Perrin Didier, J.-C. Bénézet, S. Mani, F. Coiffier, et al.. Reprocessing of artificial UV-weathered wood flour reinforced polypropylene composites. *Polymer Degradation and Stability*, 2015, 120, pp.313-327. 10.1016/j.polymdegradstab.2015.07.013 . hal-02900379

HAL Id: hal-02900379

<https://imt-mines-ales.hal.science/hal-02900379>

Submitted on 25 May 2021

HAL is a multi-disciplinary open access archive for the deposit and dissemination of scientific research documents, whether they are published or not. The documents may come from teaching and research institutions in France or abroad, or from public or private research centers.

L'archive ouverte pluridisciplinaire **HAL**, est destinée au dépôt et à la diffusion de documents scientifiques de niveau recherche, publiés ou non, émanant des établissements d'enseignement et de recherche français ou étrangers, des laboratoires publics ou privés.

Reprocessing of artificial UV-weathered wood flour reinforced polypropylene composites

L. Soccalingame^a, D. Perrin^a, J.-C. Bénézet^a, S. Mani^b, F. Coiffier^b, E. Richaud^c, A. Bergeret^{a,*}

^a C2MA¹, Ecole des Mines d'Alès, 6 Avenue de Clavières, 30319 Alès Cedex, France

^b PEP, Pôle Européen de Plasturgie, Rue Pierre et Marie Curie, 01100 Bellignat, France

^c Arts et Métiers ParisTech, PIMM, CNRS, UMR 8006, 151 Boulevard de l'Hôpital, 75013 Paris, France

A B S T R A C T

This work aims to determine and understand the influence of UV weathering on the reprocessing of a wood-plastic composite (WPC), i.e. of a wood flour reinforced polypropylene (PP) composites. Two wood flour contents (10% w/w and 30% w/w) were studied in comparison with neat PP. Compounds were produced by twin-screw extrusion. Then, ISO1A “dog bone” samples were obtained by injection molding and exposed to an artificial UV weathering using a xenon arc climatic chamber in order to simulate a long-term outdoor exposure. After this weathering stage, photo-degraded samples were submitted to grinding and injection cycles and characterized through different experimental technics. The visual evolution of the surface was followed by optical microscopy and scanning electron microscopy. In order to understand the material physical degradation, the mechanical behavior was measured thanks to tensile, Charpy impact and DMTA (Dynamic Mechanical Thermal Analysis) tests. The assessment of the microstructural evolution was performed by differential scanning calorimetry (crystallinity ratio), size exclusion chromatography (average molecular weights) tests and infrared spectroscopy (chemical structure). Additional rheological tests assessed assumptions on degradation mechanisms.

Keywords:

Polypropylene
Wood flour
Biocomposites
Reprocessing
UV weathering
Microstructure
Mechanical properties
Degradation

1. Introduction

The industrial use of wood-plastic composite (WPC) is growing since several years around the world. These composites are prevalent in outdoor decking applications and concern thermoplastic polymers reinforced by wood fibers or flour. The most widespread polymer matrices are polypropylene (PP), polyethylene (PE) and polyvinyl chloride (PVC). This study will focus on wood flour reinforced polypropylene composites. Assessing WPC recycling capability is up to now a challenging economic and scientific goal. According to Winandy et al. [1], the main issues that need to be studied to handle the recycling of these materials are the raw material effects, processing behaviors and the evolution under specific environmental conditions.

Concerning the raw material effects, some authors examined

the effect of virgin versus recycled raw materials for both phases – matrix and reinforcement – on the properties of WPCs. Youngquist et al. [2] and Adhikari et al. [3] investigated both recycled and virgin HDPE matrices with wood flour. They did not show any significant variation in the WPC mechanical and physical properties between virgin polyethylene (HDPE) and post-consumer HDPE. The study from Youngquist et al. [2] compared hemlock fiber with demolition wood fiber and found that they were equivalent. The use of fibers from waste newspapers in PP or HDPE matrix was also investigated and reveals to provide satisfactory properties and an aptness to be reprocessed (re-extruded and injection molded) numerous times with no detrimental effects in mechanical properties. Otherwise, our previous study [4] has highlighted no significant influence of wood flour particle size or the addition of maleic anhydride grafted polypropylene (as coupling agent) on the properties after reprocessing (up to seven injection molding and grinding cycles) of wood flour reinforced polypropylene.

In connection with processing effects, the study of processing impacts on WPC properties leads to the assessment of thermal degradation of each component. This thermal degradation can

* Corresponding author.

E-mail address: Anne.Bergeret@mines-ales.fr (A. Bergeret).

¹ C2MA is a member of the European Polysaccharide Network of Excellence (EPNOE), www.epnoe.eu.

result on one hand in both cross-linking and chain scission of the polymer matrix and on the other hand in structural and chemical attrition of the wood flour. These phenomena can occur at different levels and have more or less impact on the global composite properties. Since almost two decades, a large number of studies have found that successive processing cycles induce a polymer matrix chain scission indicating a thermal oxidation during reprocessing in both neat and reinforced polypropylene and polyethylene composites. This behavior is induced by a polymer chain degradation due to a severe thermal and stress cycle during the process [4–13]. It was reported that PP is notably less stable than PE [14]. Otherwise, Migneault et al. [15] compared extrusion and injection molding processes for HDPE with wood flour. They observed better physical and mechanical properties for injection than extrusion. The injection process results in better fiber alignment in the main flow direction, as polymer-rich surfaces may prevent some defects such as exposed fibers and voids. Moreover, this kind of polymer layer hinders water absorption and swelling and promotes a better durability. Concerning natural filler degradation, some papers focused on vegetal fibers or flour behavior during processing. Reprocessing induces a decrease in the fiber size because of high shear rates during process. However, this fiber structural breakdown may have a low impact on the mechanical properties of the composite [4,16–18]. Otherwise micromechanical tests by nanoindentation carried in a previous study [4] have shown a progressive increase of wood particle intrinsic hardness through the processing cycles. This phenomenon is explained by a possible degradation or migration of hemicellulose and lignin components.

As summarized by Azwa et al. [19] the number of papers published on the degradation of synthetic and natural fiber reinforced polymer composites due to environmental parameters raised significantly for the past 10 years. Environmental parameters concern mainly fungal decay, UV and moisture exposures. Pendleton et al. [20] observed that mycelium decay on wood flour reinforced HDPE induces surface erosion and decreases global mechanical properties by growing mainly in the interfacial gaps between the wood and the thermoplastic matrix. Generally, the higher the wood fiber content, the greater is the potential for fungal decay to occur [21]. Another major degradation factor of WPCs is outdoor exposure which is mainly characterized by a combined UV/humidity exposure. Weathering performed on WPCs generally induced a mechanical property alteration due to oxidation reactions (chain scission, recombination, crosslinking), a surface erosion with flouring effect, a surface yellowing and bleaching, a surface cracking, crystallinity changes and dimensional instability (swelling and shrinking) [22,23]. About vegetal fiber aging, it was found that two successive reactions may occur: i) formation of paraquinone chromophoric structures generated by oxidation and chain scission of lignin, causing yellowing, ii) conversion of paraquinone into hydroquinone, causing bleaching [22,24]. Recent papers from Peng et al. [25,26] highlighted the positive role of lignin: it is the main component causing WPC discoloration but limits mechanical degradations by acting as an antioxidant. On the contrary, cellulose is less sensitive to bleaching but induces more deterioration in mechanical properties.

Few studies handled the impact of weathering on WPC recycling. In a review from Kazemi-Najafi et al. [27], numerous studies were cited concerning the use of post-consumer PP or PE as a polymer matrix for WPCs. It was found that the recycling potential is high in WPCs as the global mechanical properties are not much impacted with recycled waste plastics as already cited above. Concerning PP and PE matrices, weathering degradation generally consists in an oxidation phenomenon caused by high temperature and/or UV exposures resulting in chain scission and/or crosslinking.

Crosslinking degradation was reported for various polyethylene studies under UV weathering. It was shown that this phenomenon induces a lower melt flow index compromising strongly the aptness of the material to be reprocessed because crosslinked polymers do not melt [27]. On the contrary, chain scissions induce a decrease in global mechanical properties and in polymer viscosity. Furthermore, the oxidation of PP or PE leads to carbonyl and hydroxyl groups which are polar groups. It was noticed that these polar groups improve compatibility between polar fillers such as lignocellulosic fibers, bettering interface between untreated natural fibers and polymer matrix [27].

Otherwise, Jansson et al. [28] studied the thermal oxidation impact on reprocessing cycles of post-consumer PP/PE copolymers. A zigzag shaped elongation-at-break curve was observed, i.e. the elongation drops considerably after each aging step and returns approximately to the initial value after extrusion. A combination of three mechanisms was proposed: i) changes in the crystallinity ratio, ii) degradation located at the surface and iii) dilution of degraded polymer chains after re-extrusion. Combining extrusion and aging degrades stronger than aging or reprocessing does separately. Luzuriaga et al. [29] used the same type of methodology with various polymers and an accelerated UV weathering. This study showed that melt flow indexes (MFI) of PP and HDPE are highly impacted by reprocessing combined with UV aging. HDPE presented a zigzag MFI curve which evidenced a competition between chain scission and crosslinking phenomena. In contrary, PP indicated a progressive increase in MFI meaning that a chain scission occurred during both aging and reprocessing without the shorter polymer chains being diluted. Afterward, a similar conclusion were expressed by both Jansson et al. [28] and Luzuriaga et al. [29]: as the content and the type of additives contained in commercialized polymer granules are frequently unknown, a complete understanding of the results remains elusive.

Additionally, a review from Vilaplana and Karlsson [30] stated that the quality of recycled plastics depends, among other parameters, on the degree of degradation (chemical and physical evolutions). Finally, this background review highlighted that recycling involves a polymer degradation which is not completely understood. To bring new elements of understanding to WPC recycling, this paper purposes to characterize and understand the influence of UV weathering on the potential of reprocessing of spruce wood flour reinforced PP composites. The evolution of the surface aspect and mechanical properties was followed through different technics. Extensive experiments were performed to assess and understand the evolution of viscoelastic properties and macromolecular chain behavior. Additional rheological tests assessed assumptions on degradation mechanisms by using the Cole–Cole model dedicated to investigate the polymer microstructure at the molten state. Surface chemical structure was also analyzed by infrared spectroscopy.

2. Materials & methods

2.1. Raw materials

Polypropylene (PP) used in this study is a standard homopolymer PP H733-07 grade supplied by Braskem Co. (Brazil) with a melt flow rate of 7.5 g/10 min (230 °C, 2.16 kg) according to ISO 1133 standard. Maleic anhydride grafted polypropylene (MAPP) with a 1% w/w grafting rate is used as coupling agent and provided by Arkema Co. (France) under the trademark Orevac® CA100. It was dry-mixed before processing at 3% w/w of the PP. The wood flour is based on spruce wood with a particle size included in the 200 µm–500 µm range and was purchased from AFT Plasturgie Co. (France). The wood flour was added at 10% w/w and 30% w/w in the matrix.

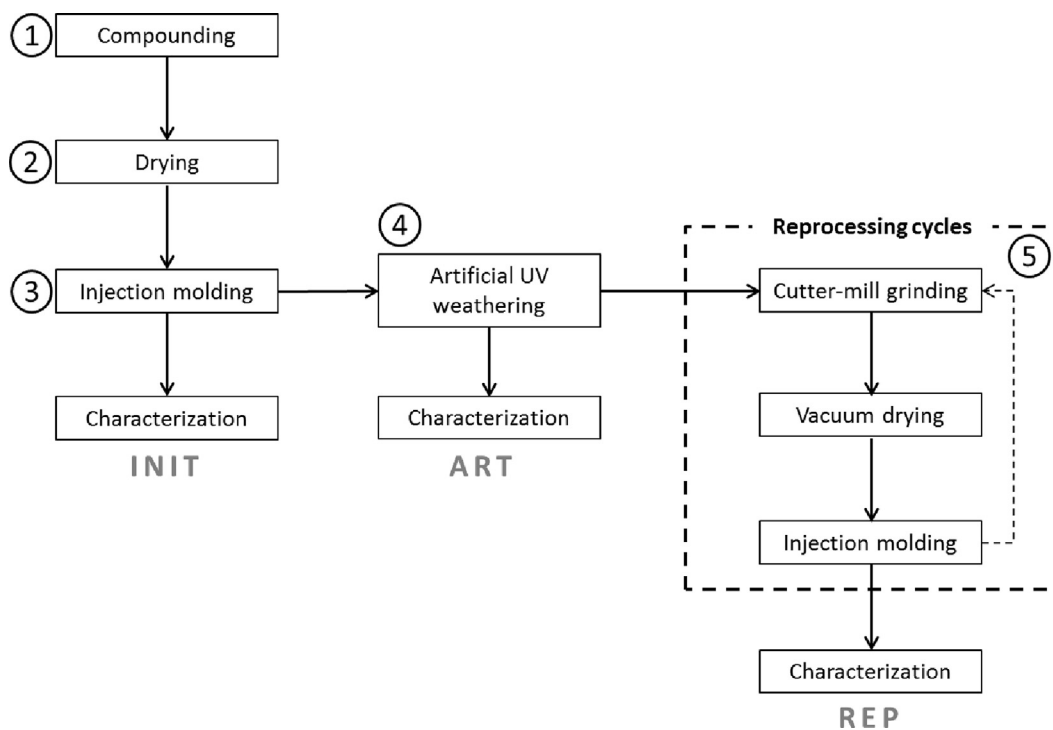


Fig. 1. Stages of the weathering and reprocessing method.

2.2. Processes and artificial weathering

The processing methodology is summarized in Fig. 1 and the successive stages are detailed below.

The PP matrix and the wood particles are mixed together in an Evolum[®] HT32 Clextal (France) co-rotating twin-screw extruder (step ①). Its L/d ratio is 44 with a 32 mm screw diameter and a 1408 mm screw length. Temperature is set at 180 °C along the barrel. The screw speed is arbitrarily fixed at 200 rpm with a total feeding rate of 14 kg/h. The extruder is equipped with a double extrusion die with a diameter of 4 mm. The two extruded compound rods are cooled into water and granulated. Pellets are kept 4 h at 35 °C (step ②) in an air-pulsing Piovan[®] dryer.

The pellets are injection molded to produce ISO1A samples on a Krauss-Maffei KM50-T180CX. The temperature is fixed at 180 °C along the barrel. The mold is kept at 30 °C by a water cooling system. The plasticization and injection speeds are set respectively at 60 rpm and 60 cm³ s⁻¹. The samples are injected to obtain dog-bone samples ISO1A according to ISO 527-2 (step ③). Samples are characterized at this step to evaluate their initial stage (INIT).

ISO 1A samples are exposed according to EN ISO 4892-2 standard in a xenon arc chamber Weather-Ohmeter (WOM) from Atlas Co. with a 3500 W lamp. The lamp characteristics report an irradiance of 60 W/m² in the range of 300 nm–400 nm (UV radiations). A 120-min cycle was applied and repeated 168 times for total exposure duration of 14 days. This cycle is composed of two stages: a 102-min of UV exposure at 60 °C and 65 ± 5%HR followed by an 18-min water spraying (step ④). As reported in Table 1 for three outdoor exposure benchmark sites [31], these conditions equal to a range of 2–3 months of natural exposure considering UV radiations only (300–400 nm).

Aged samples are characterized (ART stage), then grinded and injected to simulate recycling (step ⑤). The grinding process is performed in a RETSCH SM300 cutter mill to obtain flakes. The grinding process is carried out at 700 rpm at room temperature with an 8 mm sieve. The flakes are stored at room temperature and

vacuum dried overnight at 80 °C before injection molding. This protocol is accomplished 2 times (REP stage). Samples used in this study are detailed in Table 2.

2.3. Characterization of surface evolution

2.3.1. Optical microscopy

Color and texture changes of the sample surface are visually assessed with a Leica WILD M10 optical microscope. Pictures are taken at ×10 and ×50 magnifications with a Leica DFC 420 camera. Pictures from a same material are taken with the same light intensity to properly discern color changes.

2.3.2. Environmental scanning electron microscopy (ESEM)

Environmental scanning electron microscopy (ESEM) is performed using a Quanta FEG 200 set-up in order to have a better visual appreciation of the surface degradation. Surfaces were carbon coated beforehand. Samples were observed on their aging-exposed surface at 15 kV.

2.4. Mechanical characterization by solid-state static and dynamic tests

2.4.1. Tensile tests

Tensile characterizations are carried out at 23 °C ± 2 °C and 50% ± 10%HR according to the ISO 527 standard. A Zwick[®] 1455 model apparatus is used with a 20 kN load cell and a Clip-On extensometer for displacement measurements during modulus tests. The crosshead speed is set at 1 mm/min for the tensile modulus measurements, 50 mm/min for the break property measurements. Five measurements are carried out for modulus measurements and for strength and elongation at break measurements.

2.4.2. Charpy tests

Impact strength is measured with a Charpy pendulum impact tester Zwick[®] 5102. The tests are performed at 23 °C ± 2 °C and

Table 1
Comparison of natural weathering with xenon arc chamber Weather-Ohmeter (WOM) artificial weathering [31].

Location	Climate type	Average solar radiant exposure in one year		Equivalent duration for the WOM exposure ^c	
		Total ^a	UV ^b	in days	in months
Florida, USA	Sub tropical	6588 MJ/m ²	280 MJ/m ²	95	3.2
Bandol, France	Mediterranean	5500 MJ/m ²	382 MJ/m ²	69	2.3
Arizona, USA	Desert	8004 MJ/m ²	334 MJ/m ²	79	2.6

^a Solar radiation measured between 300 nm and 3000 nm.

^b Solar radiation measured between 300 nm and 400 nm.

^c Regarding UV radiations only, according to 168 cycles of 120 min (EN ISO 4892-2).

Table 2
Designation of the studied materials.

Wood flour content by weight	Unaged INITIAL state	ARTificial UV aged	REProcessed after artificial UV aging
0%	PP _{INIT}	PP _{ART}	PP _{REP}
10%	PP/WF10 _{INIT}	PP/WF10 _{ART}	PP/WF10 _{REP}
30%	PP/WF30 _{INIT}	PP/WF30 _{ART}	PP/WF30 _{REP}

50% ± 10%HR according to the ISO 179 standard and repeated for ten samples. A 4 J pendulum is chosen. The unnotched samples are sawn from the injected ISO1A dog bone samples to obtain samples with 80 × 10 × 4 dimensions.

2.4.3. Dynamic Mechanical Thermal Analysis (DMTA)

A DMA 50 apparatus is used to DMTA tests on 4 mm × 10 mm × 35 mm samples sawn from ISO 1A samples. The samples are stressed in tensile mode with a 1 Hz frequency. A temperature sweep is carried out from −20 °C to 120 °C with a temperature ramp of 2 °C/min. The relaxation behavior is evaluated in order to characterize the polymer matrix degradation. Two samples are tested for each studied material.

2.5. Characterization of the polymer microstructure

2.5.1. Differential scanning calorimetry (DSC)

The melting and crystallization behaviors of biocomposites and neat polymer are assessed through differential scanning calorimetry (DSC) using a Q100 TA Instruments[®] equipped with a cooling attachment, under a nitrogen atmosphere. Two heating steps interspersed with a cooling step from 30 °C to 220 °C at a constant rate of 5 °C min^{−1} are carried out. The sample weights are approximately 5 mg. They are analyzed in standard aluminum DSC pans. At least, two specimens are used for each test to ensure reproducibility. Melting enthalpy is obtained from the 1st and the 2nd heating steps. The intermediate cooling step was conducted at 5 °C min^{−1}. The crystallinity χ_c was calculated according to the Equation (1):

$$\chi_c = \frac{\Delta H_m}{W \times \Delta H_{m100\%}} \times 100 \quad (1)$$

where ΔH_m is the melting enthalpy of the composite, W is the PP content by weight in the composite and $\Delta H_{m100\%}$ is the melting enthalpy for a 100% crystalline PP polymer. It is considered equal to 209 J/g [32].

2.5.2. Rheological tests

The evolution of the rheological material properties directly reflects changes in molecular parameters such as the chain scission and recombination or crosslinking phenomena. Thus, dynamic rheological measurements are carried out to assess the change in complex viscosity using an ARES rheometer (Rheometric

Scientific[®]). The melt viscoelasticity tests in oscillatory shear mode are performed with parallel plate equipment at a fixed temperature of 180 °C. The plate diameter is 25 mm and the gap between them was 1 mm. A frequency sweep was carried out from 0.1 to 100 rad s^{−1} for each experiment.

The samples are cut at the extremities of the injected dog-bone samples and placed between the parallel plates. Once the fixed temperature is reached, the gap is controlled at 1 mm. Then, the molten excessive matter is removed and the test is started. At least three tests are performed for each material.

Additionally, to determine information about the polymer microstructure at the molten state, the Cole–Cole model was used. The Cole–Cole diagram representation consists in plotting the imaginary part η'' of the complex viscosity η^* as a function of its real counterpart η' . If the studied polymeric material obeys the Cole–Cole model, plotted data form a circular arc described as follow (Equation (2)) [33]:

$$\eta^*(i\omega) = \frac{\eta_0}{1 + (i\omega\lambda)^{(1-\alpha)}} \quad (2)$$

where ω is the test pulsation, λ is the macromolecular chain relaxation time, α is the dispersion parameter and η_0 is the newtonian viscosity. Thus, the complex viscosity and the concomittant molecular motions are dependent on frequency for the mechanical relaxation of stress. The real and imaginary part of the complex viscosity as modeled by the Cole–Cole function can be derived from these two following Havriliak and Negami equations (Equations (3) and (4)) [34]:

$$\eta'(\omega) = \frac{\eta_0(1 + (\omega\lambda)^{(1-\alpha)} \sin(\frac{\alpha\pi}{2}))}{1 + 2(\omega\lambda)^{(1-\alpha)} \sin(\frac{\alpha\pi}{2}) + (\omega\lambda)^{2(1-\alpha)}} \quad (3)$$

$$\eta''(\omega) = \frac{\eta_0(\omega\lambda_0)^{(1-\alpha)} \cos(\frac{\alpha\pi}{2})}{1 + 2(\omega\lambda_0)^{(1-\alpha)} \sin(\frac{\alpha\pi}{2}) + (\omega\lambda_0)^{2(1-\alpha)}} \quad (4)$$

By fitting these two equations with experimental data at each test frequency by a least-square procedure, one can determine the relaxation time λ , the dispersion parameter α and the newtonian viscosity η_0 by extrapolation to low frequencies. These three parameters are representative of the polymer mobility and the polymer chain length above melting temperature.

2.5.3. Size exclusion chromatography (SEC)

Size-exclusion chromatography is performed in a high temperature gel permeation chromatograph to determine the evolution of the average molecular weights in weight and in number and the polydispersity index of PP. Fragments are cut in the injected samples on the exposed surface and solubilized into 1,2,4-trichlorobenzene (Chromasolv, Sigma–Aldrich[®]) at a concentration of 1 mg mL^{−1}. The eluent was stabilized with 0.03 wt% of 2,6-

di-tert-butyl-4-methylphenol (BHT, Fluka) to stabilize the polymer against oxidative degradation. These solutions are agitated during 15 min at 150 °C and, then filtered before test. The tests are carried out on a PL-GPC 220[®] from Agilent Technologies equipped with a guard column and two columns branded PLGel Olexis[®] as well as a refractive index detector. The temperature was set at 135 °C, and the flow rate was 1 mg mL⁻¹. The calibration curve was established from four Polystyrene Shodex[®] narrow standards of respective molecular weights of 1.47·10⁶, 2.57·10⁵, 4.65·10⁴ and 7.21·10³ g mol⁻¹. Results were then corrected using the so-called “universal calibration”, based on Mark–Houwink’s relationship.

2.5.4. Infrared spectroscopy

Infrared spectroscopy is carried out to assess the evolution of specific chemical groups during the degradation phenomenon induced by weathering and reprocessing. Spectra from weathered materials are obtained on the exposed surface. A spectrometer IFS66 from Bruker[®] is used in ATR mode (Attenuated Total Reflection). The spectra are measured from 400 cm⁻¹ to 4000 cm⁻¹ with a 2 cm⁻¹ resolution. The mentioned peaks were normalized with the 2915 cm⁻¹ attributed to a C–H stretching band of methylene groups CH₂. This band is chosen as a reference because it changed minimally during weathering [35].

3. Results and discussion

3.1. Evolution of the surface aspect

The sample surface aspect is presented on Table 3 for PP, PP/WF10 and PP/WF30 respectively as a function of the different stages (INIT, ART and REP). No specific visual degradation can be observed for PP samples.

On the contrary, wood composites present very strong visual surface variations. For both PP/WF10 and PP/WF30, weathering induces a wood particle bleaching and a protrusion of these particles at the surface with many cracks. It was shown that wood bleaching during weathering is mainly due to the lignin component [25,26]. Absorption of UV light initiates the photochemical reactions of wood surfaces leading to the formation of aromatic and other free radicals, which causes the degradation of lignin and photo-oxidation of cellulose and hemicelluloses, effectually causing discoloration. This discoloration of wood surfaces results from the loss of methoxyl content of lignin photo-dissociation of carbon–carbon bonds and formation of carbonyl-based chromophoric groups like ortho- and para-quinone structures [36,37]. Additionally, the PP/WF30 presents a flouring phenomenon (not present on PP/WF10) as the sample crumbles on the exposed surface.

After reprocessing, the composite surfaces recover a glossy aspect thanks to injection molding process with no protrusion of the wood particles. The bleached aspect has disappeared but the global color is slightly darker than the initial state.

Fig. 2 presents ESEM pictures performed after weathering (ART) and after reprocessing (REP) on the PP/WF10 and PP/WF30 surfaces for a better contrast. Pictures at the initial state displays a very smooth surface thanks to injection molding whatever the considered material so, they are not shown here. After weathering, PP/WF10_{ART} exhibits numerous micro-cracks and the protrusion of some wood particles at the surface. It can be found with a higher magnification that some parts of the PP matrix are detaching from the sample. Concerning PP/WF30_{ART}, a high wood content is observed at the surface with many cavities around the wood, matching with the PP debonding. This debonding must be favored by the water spraying during the weathering cycles that washes the surface. After reprocessing, both materials display a smoother surface with some remaining asperities.

3.2. Evolution of mechanical behavior

Fig. 3 shows tensile properties of all studied material at each stage. Elastic modulus values present an expected increase with the addition of wood flour at the initial stage. For each material, the artificial weathering induces a slight increase (3%–9%) which can be explained by the promotion of PP crystallization induced by shorter macromolecular chains resulting from a predominant chain scission phenomenon occurring during the weathering [38].

Then, the reprocessing step after weathering brings modulus values down, lower than the initial state for PP and PP/WF10. Otherwise, PP/WF30 modulus turns back to its initial value and shows the least variations. Lignin is supposed to play a positive role in retarding photodegradation of composites due to its structure of hindered phenols [39,40]. Opacification of the material can also be an important factor to limit the light scattering.

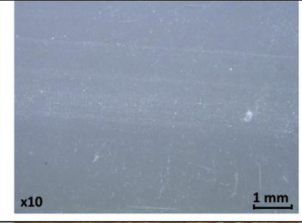
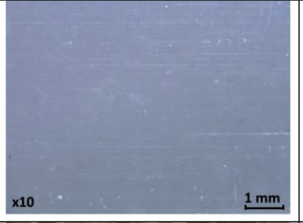
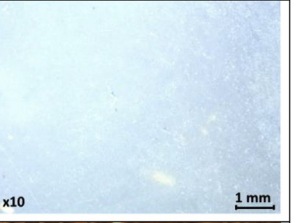
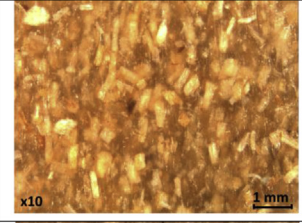
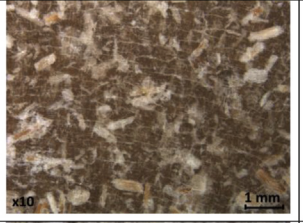
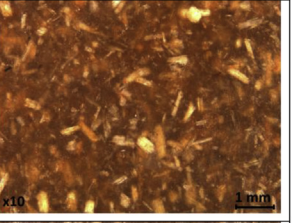
Considering the yield strength, PP/WF10 does not present a higher value than PP contrary to PP/WF30 at the initial stage. It may be explained by an insufficient wood flour content to reveal a significant improvement in the yield strength for PP/WF10 despite the addition of the MAPP coupling agent. Tensile yield strengths show a very stable behavior through the successive ART and REP stages for each material.

Concerning the tensile elongation at yield, the addition of wood flour shows an expected decrease at the initial stage correlating the elastic modulus tendency. For each material, the artificial weathering induces a 50% decrease. This decrease can be explained by a strong chain scission phenomenon correlating assumptions from modulus evolution [38]. Then, the reprocessing step after weathering turns elongation at yield values back to the initial state for PP and PP/WF composites.

Results from un-notched Charpy tests are plotted in Fig. 4. One can see that PP does not break at the initial state thanks to its ductile property. The impact strength decreases with the addition of wood flour in agreement with the modulus and the elongation at yield variations. PP does break after the weathering step but return to its ductile state after reprocessing. Concerning PP/WF10, the same tendency is observed with a decrease in impact strength after weathering, and a “regeneration” of impact properties after reprocessing. As observed for tensile characteristics, PP/WF30 is not really sensitive to weathering and reprocessing. The decrease in impact strength is attributed to a chain scission degradation and an increase in crystallinity. These global trends are similar to the behavior observed for tensile modulus and deformation. As seen before, the addition of wood flour reduces the ductility of PP and reduces the sensitivity against degradation by weathering and reprocessing, especially for PP/WF30. It can attributed to the higher lignin content with high flour content, lignin acting as an antioxidant during weathering [25,26].

The “regeneration” tendency can be observed with the reprocessing for both mechanical technic as it enables to partially or totally recover the degraded properties such as the elastic modulus, the elongation at yield and the impact strength. This phenomenon can be explained by a competition between chain scission and recombination mechanisms as well as a transfer of degraded chains from amorphous phases to crystalline phases as related by Jansson et al. [28] and Luzuriaga et al. [29]. Indeed, as PP is a semi-crystalline polymer, one can suppose at the initial state that the most degraded chains must be chains from the amorphous phase. Consequently, rigidity and impact strength decreases with weathering but tensile strength remains unchanged. After the reprocessing step, the material is wholly molten and homogenized: degraded chains which are shorter tend to reorganize during cooling into crystalline phases while the non-degraded ones compose the amorphous phase. Afterward, degraded chains seem

Table 3
Micrographs of sample surface for neat PP and PP/WF composites at the different stages: INIT, ART and REP.

	INIT	ART	REP
Neat PP			
PP/WF10			
PP/WF30			

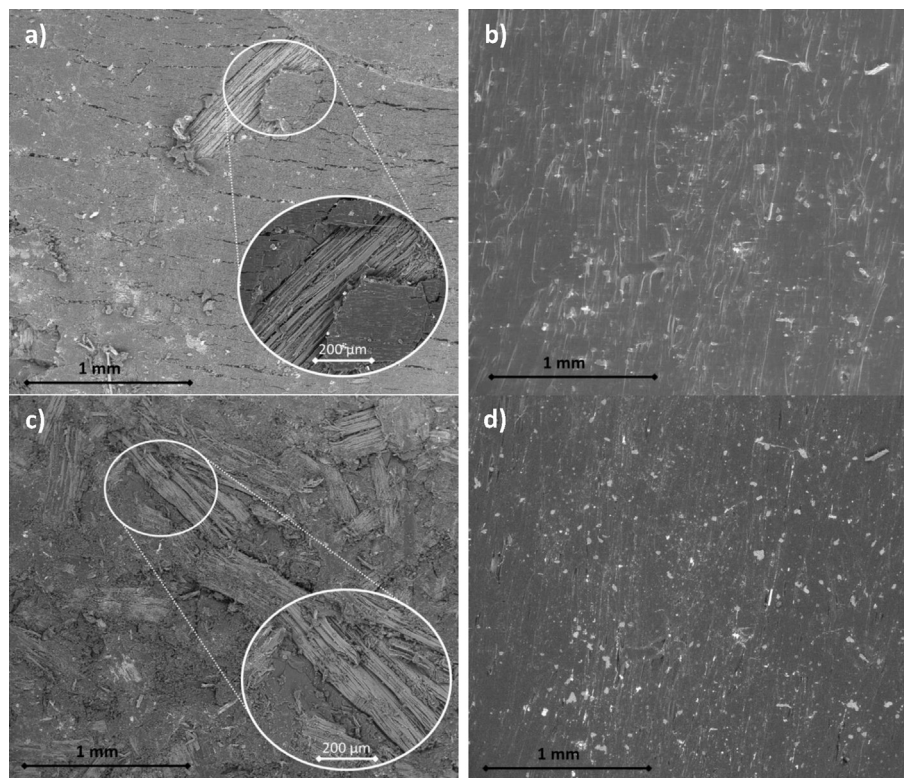


Fig. 2. ESEM pictures of the sample surface of PP/WF10_{ART} (a), PP/WF10_{REP} (b), PP/WF30_{ART} (c) and PP/WF30_{REP} (d).

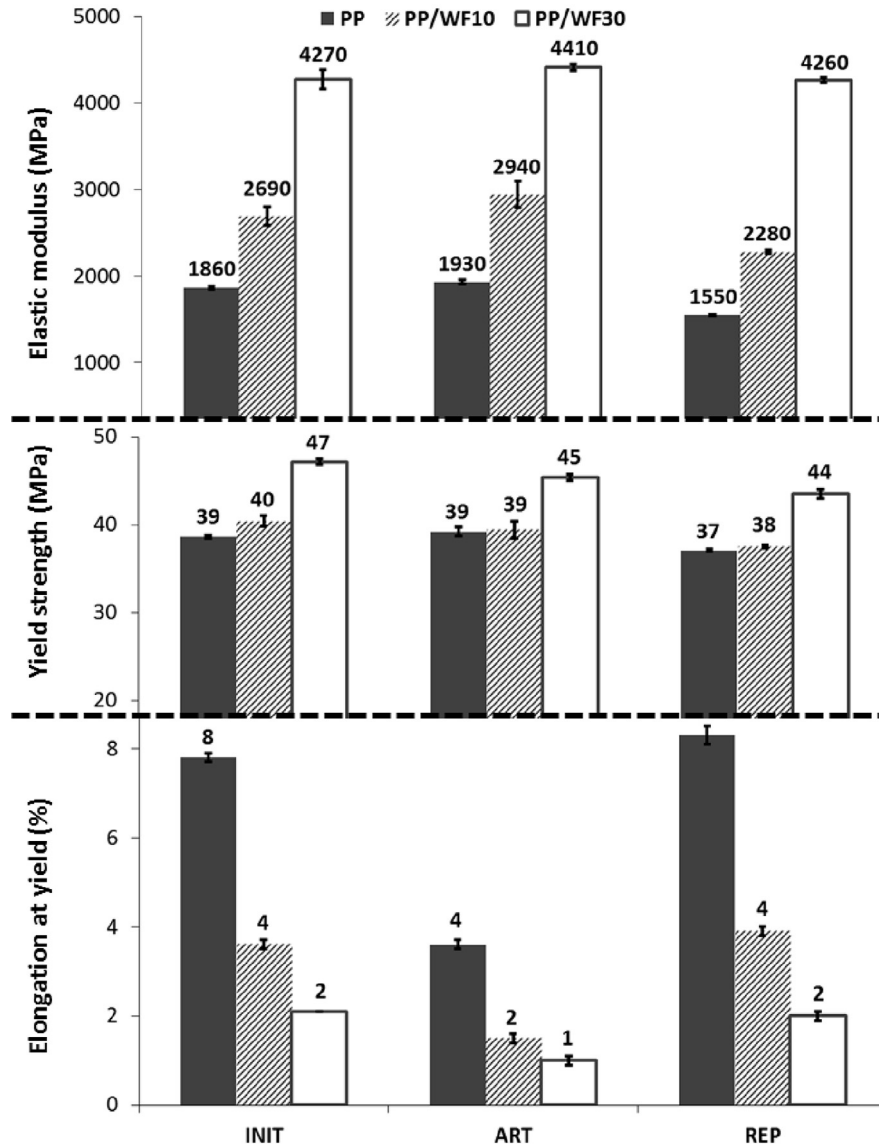


Fig. 3. Tensile properties (elastic modulus, yield strength, elongation at yield) of PP and PP/WF composites at the initial state (INIT), at the weathered state (ART), at the reprocessed state after weathering (REP).

to show a weak effect on the reprocessed material mechanical properties.

To consolidate this hypothesis, DMTA (Dynamic Mechanical Thermal Analysis) tests are carried out to assess the damping factor $\tan(\delta)$ as a function of temperature as shown on Fig. 5 for PP and PP/WF composites. In the case of semi-crystalline polymers such as PP, two transition temperatures coexists. At the glassy state, $T\alpha$ matches with the chain relaxation into the amorphous phases and is related to the glass transition temperature T_g . At the rubbery state, $T\alpha_c$ matches mainly with the chain relaxation into the crystalline phases [41]. Table 4 summarizes the mean values of $T\alpha$ and $T\alpha_c$ for each material and step.

As concerns PP, $T\alpha$ peak intensity remains unchanged whatever the considered steps (INIT, ART, REP). Otherwise, a decrease in the $T\alpha$ mean value from 21.2 ± 0.5 °C (INIT) to 19.0 ± 1.5 °C after weathering (ART) is first observed and may be caused by chain scissions enabling better macromolecular chain mobility in the amorphous phase. Then $T\alpha$ increases until 23.4 ± 0.1 °C after reprocessing of weathered PP (REP) which corroborates the

hypothesis that the new amorphous phase may include non-degraded macromolecular chains with less mobility.

Concerning $T\alpha_c$, the intensities of PP_{INIT} and PP_{ART} peaks are close but a shift on the peak towards lower temperatures (from 114.0 ± 2.3 °C to 108.0 ± 1.2 °C) can be observed. On the contrary, PP_{REP} shows an increase in peak intensity with a lower temperature (101.8 ± 0.9 °C) compared to PP_{ART} indicating a degradation of the crystalline phase chains. Indeed, these crystalline chains are shorter and present a higher relaxation level because of their higher mobility.

As concerns the wood flour reinforced composites (PP/WF10 and PP/WF30), they both show a lower $T\alpha$ at the initial state (20.0 ± 1.8 °C and 17.2 ± 2.8 °C for PP/WF10 and PP/WF30 respectively compared to 21.2 ± 0.5 °C for PP_{INIT}) possibly because of the presence of unreacted MAPP which plasticizes the PP matrix. Concerning PP/WF10, the global ART damping factor is slightly lower than the INIT one. Moreover, the $T\alpha$ values show a decrease from 20.0 ± 1.8 °C to 17.0 ± 0.4 °C due to chain scissions during weathering as already observed for neat PP. After reprocessing, an increase of $T\alpha$ from 17.0 ± 0.4 °C to 23.9 ± 0.8 °C is also observed

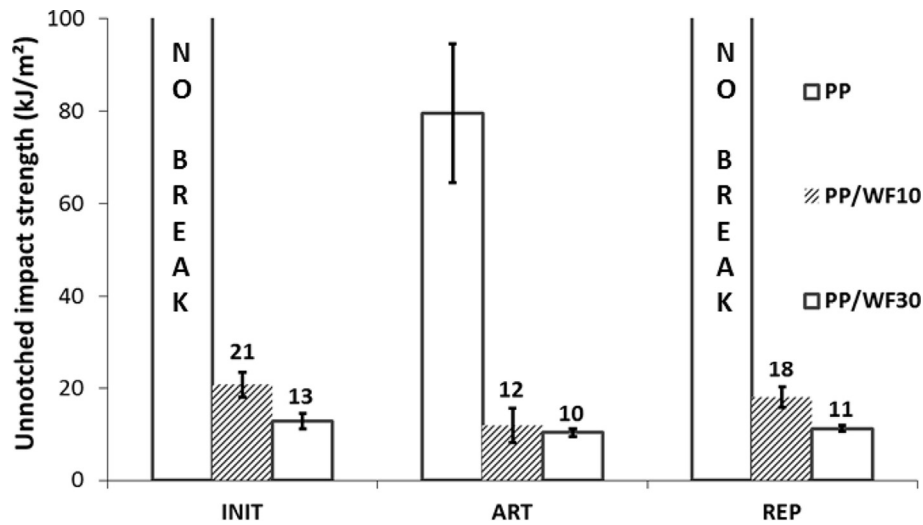


Fig. 4. Un-notched impact strength by Charpy tests of PP and PP/WF composites at the initial state (INIT), at the weathered state (ART), at the reprocessed state after weathering (REP).

and corroborates the PP results and the “regeneration” hypothesis. PP/WF30 presents a similar tendency.

Some $T_{\alpha c}$ values are not measurable (noted N.D.) as it was not detected under these test conditions because the signal amplitude is too low in the range of 100–120 °C. However, it increases from 106.9 ± 2.5 °C (INIT) to 104.4 ± 0.1 °C (REP) revealing a possible degradation of crystalline chains. Concerning PP/WF30, no

significant variation of the damping curve is observed through the steps. Moreover T_{α} peak amplitude is very low, that can be explained by the high wood content strongly limiting damping mechanisms by particle–particle frictions, particle–polymer frictions [42], and good interface between the natural filler and PP as MAPP has been added [43]. It matches previous tendencies observed for tensile and Charpy tests.

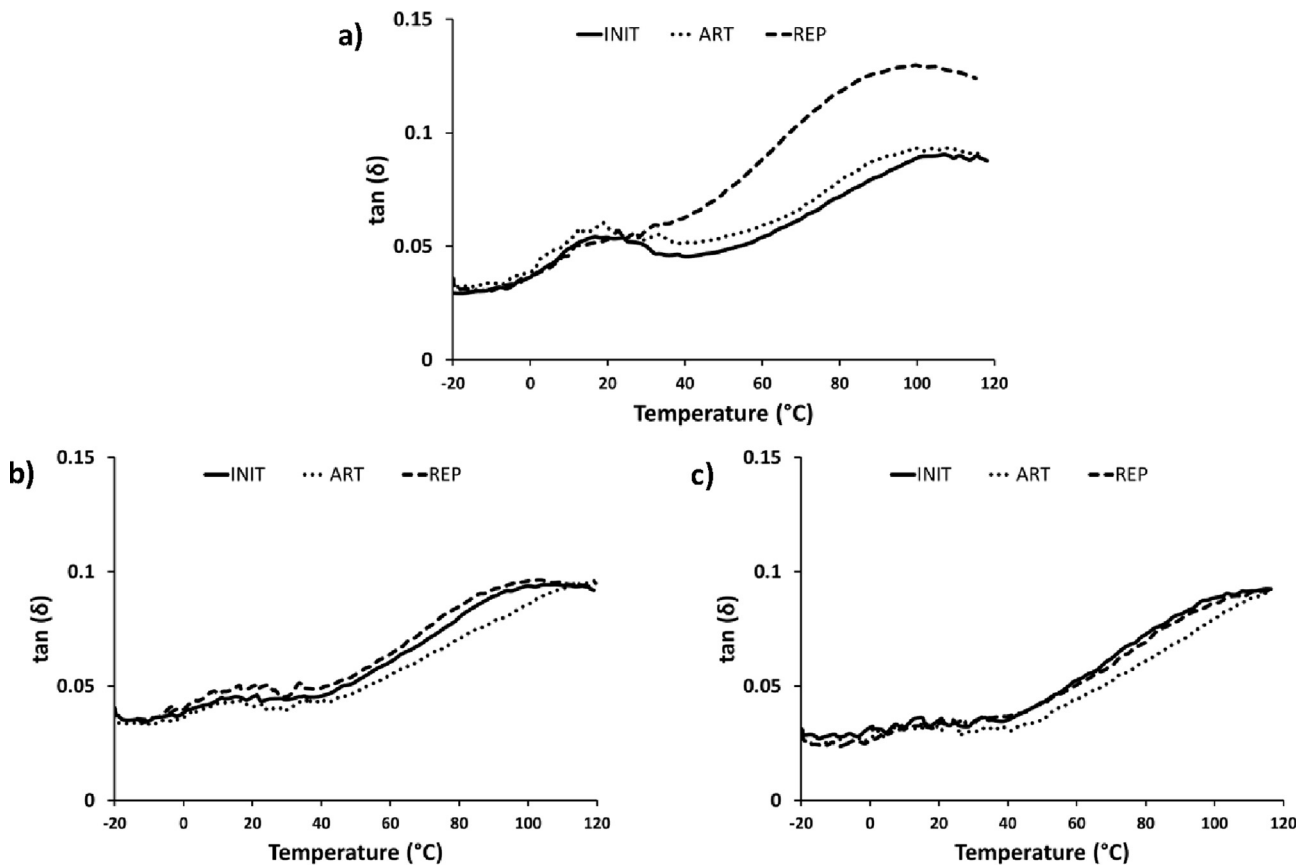


Fig. 5. DMTA results: damping factor $\tan(\delta)$ as a function of temperature for PP (a), PP/WF10 (b) and PP/WF30 (c) at the initial state (full line), at the weathered state (dotted line), at the reprocessed state after weathering (dashed line).

Table 4

Relaxation temperatures $T\alpha$ and $T\alpha_c$ measured by DMTA tests (N.D.: not detected) for PP and PP/WF composites at the initial state (INIT), at the weathered state (ART), at the reprocessed state after weathering (REP).

Materials	$T\alpha$ (°C)		$T\alpha_c$ (°C)	
PP _{INIT}	21.2	±0.5	114.0	±2.3
PP _{ART}	19.0	±1.5	108.0	±1.2
PP _{REP}	23.4	±0.1	101.8	±0.9
PP/WF10 _{INIT}	20.0	±1.8	106.9	±2.5
PP/WF10 _{ART}	17.0	±0.4	N.D.	N.D.
PP/WF10 _{REP}	23.9	±0.8	104.4	±0.1
PP/WF30 _{INIT}	17.2	±2.8	N.D.	N.D.
PP/WF30 _{ART}	11.6	±0.6	N.D.	N.D.
PP/WF30 _{REP}	17.9	±1.4	N.D.	N.D.

3.3. Evolution of the polymer microstructure

3.3.1. Crystallinity variations

The crystallinity percentages are calculated from the melting enthalpy on the first and the second heat ramp for the PP/WF composites. The results are gathered in Table 5. As the melting enthalpy measured during the first heat ramp is related to the initial crystallinity, it depends on the thermal background of the sample i.e. the aging and/or reprocessing step. It can be observed a 4% increase in the crystallinity ratio from $49.4 \pm 0.3\%$ to $53.2 \pm 2.2\%$ and from $57.1 \pm 4.5\%$ to $60.9 \pm 3.1\%$ for PP/WF10 and PP/WF30 respectively after the artificial weathering stage (ART) which is attributed to a chain scission as mentioned before [38]. It matches well with observations from mechanical properties such as elastic modulus, elongation at yield and impact strength. After reprocessing (REP), this crystallinity returns close to its initial value.

Concerning results from the second heat ramp which are more representative of the polymer state, a slight increase of the crystallinity after weathering which remains similar after reprocessing can be highlighted. This trend is also explained by a chain scission phenomenon due to photo-degradation but the reprocessing does not furthermore significantly influence the crystallization. Variations between results from the first and second ramps can be possibly explained by the cooling ramp which limits the crystallization and deletes the thermal background. Thus, under similar cooling conditions, the second ramp shows that the PP matrix is similar for both PP/WF composites.

The photodegradation at the ART stage is prevalent in the amorphous phase and the degraded chains crystallize because of their shortness and mobility. At the REP stage, these short chains are the ones which crystallize first but their quantity did not influence the PP crystallization.

3.3.2. Chain length variations

Rheological results are plotted in Fig. 6 using a Cole–Cole diagram representation. Concerning PP (Fig. 6a), a strong drop of

Table 5

Crystallinity percentages measured by DSC tests for PP/WF composites at the initial state (INIT), at the weathered state (ART), at the reprocessed state after weathering (REP).

		Crystallinity percentages (%)			
		PP/WF10		PP/WF30	
1st heating ramp	INIT	49.4	±0.3	57.1	±4.5
	ART	53.2	±2.2	60.9	±3.1
	REP	48.9	±0.3	55.5	±3.0
2nd heating ramp	INIT	50.0	±1.4	49.5	±0.5
	ART	52.0	±1.5	52.5	±1.4
	REP	52.4	±0.3	52.1	±1.0

viscosity after weathering can be observed with chain scission phenomenon. However, the reprocessing step induces an increase which can be related to a recombination phenomenon through weathering and reprocessing. Works from Verney [44] or Askanian [45] highlighted conspicuous correlations between Cole–Cole results and degradation mechanisms during aging for numerous polymers – chain scission and cross-linking mechanisms. Verney [44] presents for UV-weathered PP films a progressive drop of newtonian viscosity and a diminishing circular arc both caused by a chain scission phenomenon.

PP/WF10 (Fig. 6b) also presents a decrease of viscosity after weathering. Nevertheless, ART and REP display very close curves. PP/WF30 (Fig. 6c) has a higher viscosity because of its high wood content and shows the clearest tendency with a progressive decrease of viscosity related only to a chain scission mechanism. Besides that, a variation in the quality of the fitting process can be observed: the PP curve fitting is excellent whereas some gaps can be observed between experimental data (in dots) and the fitted curve (in dashed line) for the PP/WF composites. It seems that the addition of wood flour modifies the rheological behavior of the PP matrix limiting its correlation to the Cole–Cole model.

Table 6 lists the parameters calculated with the Cole–Cole model as well as the average molecular weights in number (\overline{M}_n) and in weight (\overline{M}_w) and polydispersity index ($I_p = \overline{M}_w/\overline{M}_n$) measured through SEC. Concerning PP, the relaxation time λ diminishes (−49%) with weathering as expected because of chain scissions, then increases after reprocessing (+18%) showing a slight recombination mechanism. The evolution in the distribution parameter α corroborates the evolution in the polydispersity index I_p showing a wider chain length distribution after weathering then reprocessing.

At the initial stage, the wood composites exhibit much higher relaxation times (+50% for PP/WF10 and +88% for PP/WF30 composites both compared to PP) because of the presence of wood particles creating an entanglement with PP chains. They show a decrease in time relaxation related to chain scission due to weathering and reprocessing (−38% for PP/WF10_{REP} compared to PP/WF10_{INIT} and −44% for PP/WF30_{REP} compared to PP/WF30_{INIT}). The very low values of average molecular weights after weathering can be explained by the fact that analyzed fragments after UV aging are collected in the first microns at the exposed surface of the samples. After reprocessing entire dog-bone samples were grinded so these SEC data correspond to a mean value of more or less degraded areas of the materials. So, SEC values after weathering are not representative of an average chain weight of the whole material as the weathering is a surface phenomenon.

For a better visualization of the evolution of chain lengths, the Newtonian viscosity is plotted as a function of the molecular weight in weight for every material in Fig. 7. A similar evolution between PP and PP/WF10 can be observed with low variations of viscosity and partial recovery of molecular weight after reprocessing. It reveals that the addition of wood flour at 10% by weight does not significantly influence the weathering/reprocessing behavior of the PP matrix. On the contrary, at 30% by weight of wood flour, the evolution tendency is greatly modified: although the molecular weight is recovered after reprocessing, the viscosity keeps decreasing. This might be attributed to the photodegradation of lignin and hemicellulose producing low molecular weight substances which can plasticize the PP matrix.

3.4. Evolution of chemical structure

Infrared spectroscopy is used to determine changes in chemical structure of the studied materials after weathering and reprocessing. Spectra from PP and PP/WF composites were normalized on

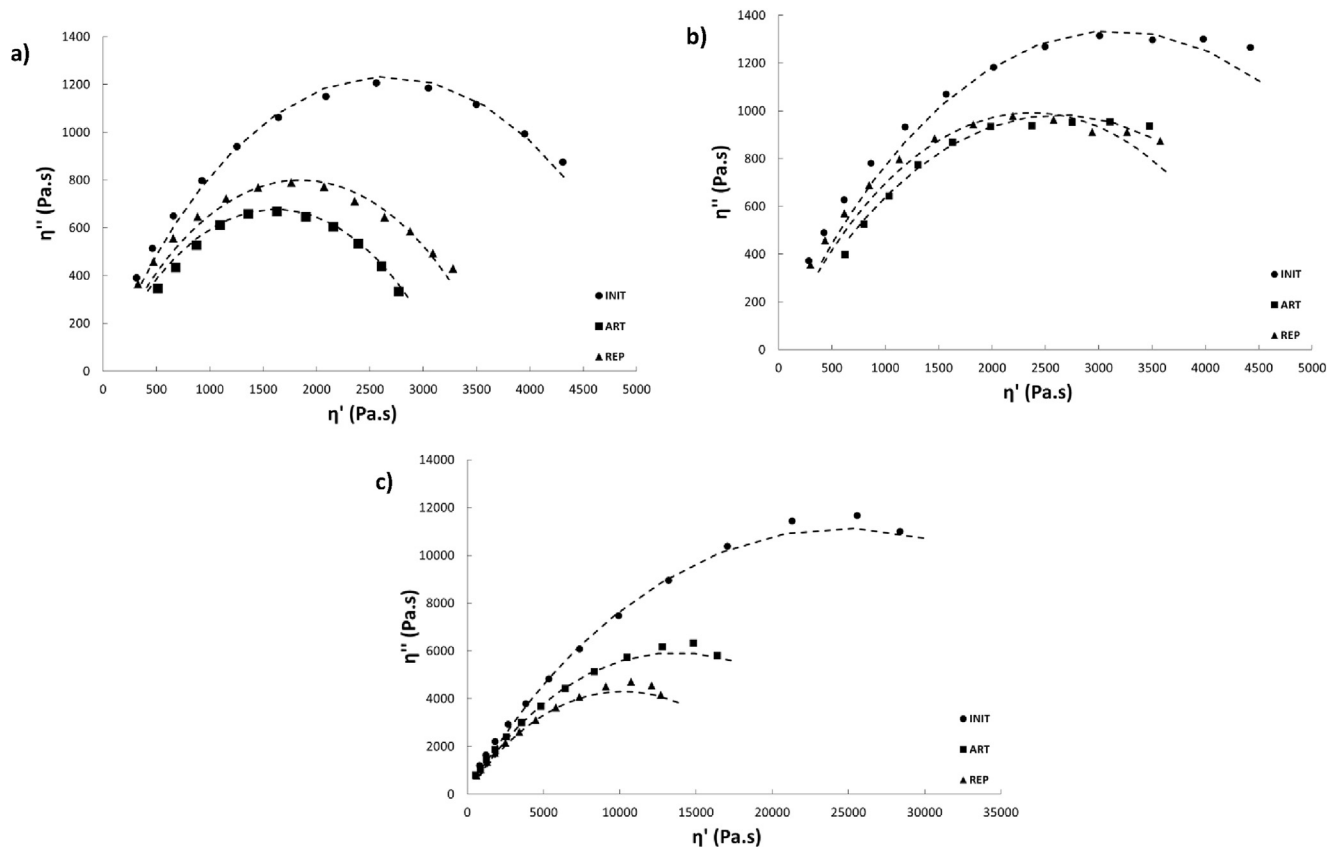


Fig. 6. Rheological results in complex plane diagrams with Cole–Cole model fitting in dashed line of PP (a), PP/WF10 (b) and PP/WF30 (c) at every stage (INIT, ART and REP) with experimental data (in dots).

Table 6
Rheological parameters and SEC results for PP and PP/WF composites as a function of the steps (INIT, ART and REP).

Materials	λ (s) ^a	α ^b	η_0 (Pa s) ^c	\overline{M}_n (g/mol)	\overline{M}_w (g/mol)	$I_p = \overline{M}_w/\overline{M}_n$
PP _{INIT}	0.61	0.45	5316	74 999	253 554	3.4
PP _{ART}	0.31	0.50	3260	6703	30 264	4.4
PP _{REP}	0.38	0.48	3700	23 129	128 080	4.8
PP/WF10 _{INIT}	1.21	0.49	6312	66 992	406 077	6.1
PP/WF10 _{ART}	1.56	0.54	5282	18 800	181 000	9.6
PP/WF10 _{REP}	0.75	0.50	4745	55 356	375 266	6.8
PP/WF30 _{INIT}	5.18	0.46	49 482	67 427	409 905	6.1
PP/WF30 _{ART}	4.19	0.48	27 380	40 647	370 752	9.1
PP/WF30 _{REP}	2.90	0.49	20 450	65 814	408 303	6.2

^a Relaxation time calculated from Cole–Cole model on experimental results at 180 °C.

^b Distribution parameter of relaxation times from Cole–Cole model on experimental results at 180 °C.

^c Newtonian viscosity calculated from Cole–Cole model on experimental results at 180 °C.

the 2915 cm^{-1} band corresponding to C–H stretching from CH_3 groups in PP which is a reference band because it changes minimally in presence of wood and during weathering [35].

Spectrum from wood flour and every material at the initial state were plotted in Fig. 8. Main bands from both wood and PP were indicated. Hydroxyl groups are preponderant in wood flour and the high wood content composite PP/WF30. In comparison with neat PP at the initial stage, the PP/WF composites show a high peak at 1650 cm^{-1} matching with a vinyl group C=C or a conjugated C–O bond [46]. One can also see an important broad peak (especially for PP/WF30) in the range of 1650–1500 cm^{-1} corresponding to C=C stretching of the lignin aromatic ring. These specific peaks can be attributed to the presence of wood flour through cellulose,

hemicellulose and lignin components. Otherwise, these wood components also contribute to the carbonyl regions in the range of 1800–1680 cm^{-1} which are specific to the PP degradation by thermal oxidation [47]. The ether vibration band from cellulose and hemicellulose at 1150–1000 cm^{-1} is high with wood flour [36]. This is greatly visible on the PP/WF30 because some wood particles are protruded from the surface.

The following investigation for weathering and reprocessing is focused on the analysis of carbonyl and vinyl groups in the range of 1800 cm^{-1} to 1680 cm^{-1} and 1650 cm^{-1} to 1500 cm^{-1} respectively [47] (Fig. 9). As concerns the effects of weathering, neat PP shows on the exposed surface an intensity increase of three main peaks: 1715 cm^{-1} attributed to carboxylic acid, 1650 cm^{-1} and 1590 cm^{-1}

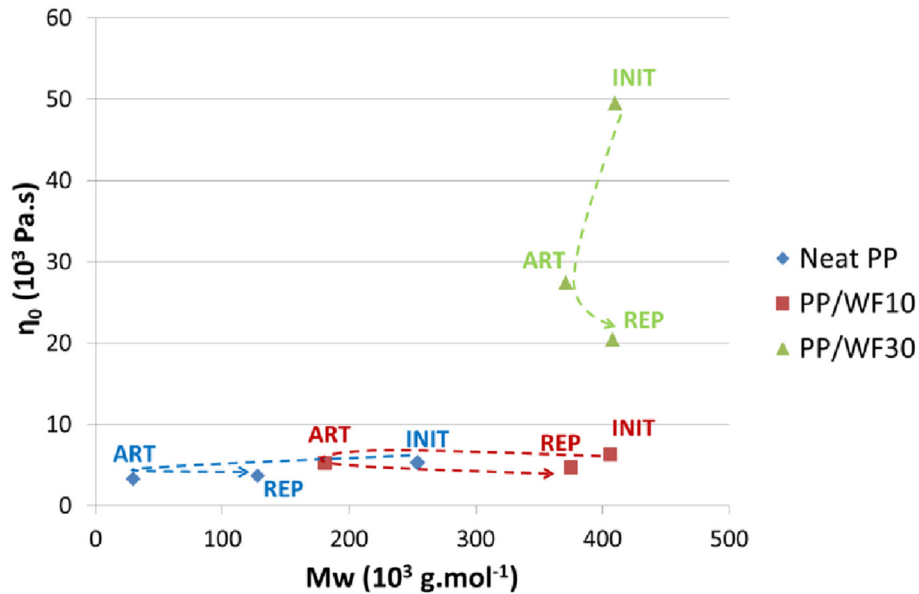


Fig. 7. Newtonian viscosity η_0 as a function of molecular weights in weight Mw for neat PP, PP/WF10 and PP/WF30 at every stage.

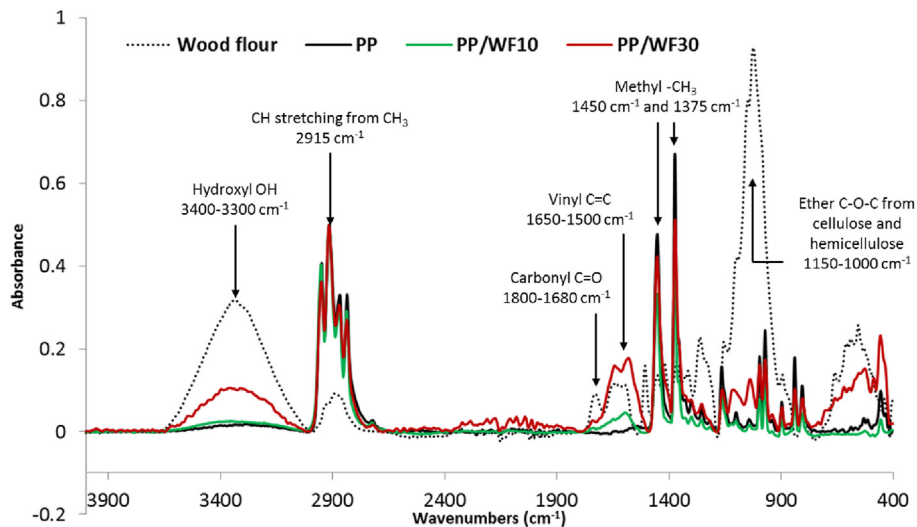


Fig. 8. Infrared spectra of wood flour and each material at the initial stage.

attributed to vinyl groups which are formed for PP photodegradation. The formation of vinyl groups is attributed to Norrish II reaction [48].

Concerning the PP/WF_{ART} composites, the appearance of a carbonyl peak located at 1715 cm^{-1} is observed after weathering. It can be attributed both to hemicellulose and PP oxidation [24,26,36,37]. Otherwise PP/WF_{30ART} displays a high intensity of the wood specific peaks (1650 and 1590 cm^{-1}) meaning that the wood content is higher on the exposed surface as already seen with the microscopic observations (Table 3) and that lignin degradation is predominant. Indeed, Peng et al. [26] mentioned the formation of carbonyl-based chromophoric groups consequently to the lignin photodegradation which causes the increase in the peak in the range of 1650 to 1633 cm^{-1} .

Nevertheless, as the PP/WF exposed surfaces were very rough because of the micro-cracking phenomenon, it does alter the infrared signal quality leading to a lot of noise.

After reprocessing, the peak intensities decrease due to the homogenization of the material through grinding and injection molding. Indeed, the degraded chains from the sample skin and the non-degraded ones from the sample core are mixed together. For neat PP, the studied peaks reach a very low absorbance level but two peaks remain visible: 1650 cm^{-1} and 1740 cm^{-1} , the second one being ascribed to ester groups. For the PP/WF composites, the wood specific band intensities diminish because protruded wood from the weathered state was mixed into the material by reprocessing.

In Fig. 10, the carbonyl absorbance at 1715 cm^{-1} is plotted as a function of the molecular weights in number and in weight for PP and PP/WF composites at the different stages. At the INIT stage, the higher \overline{M}_w values for the PP/WF composites can be attributed to possible linkages between wood components and PP. It may be due to bonds formed between hydroxyl groups from oxidized wood and oxidized PP or reactions resulting from the presence of MAPP. At

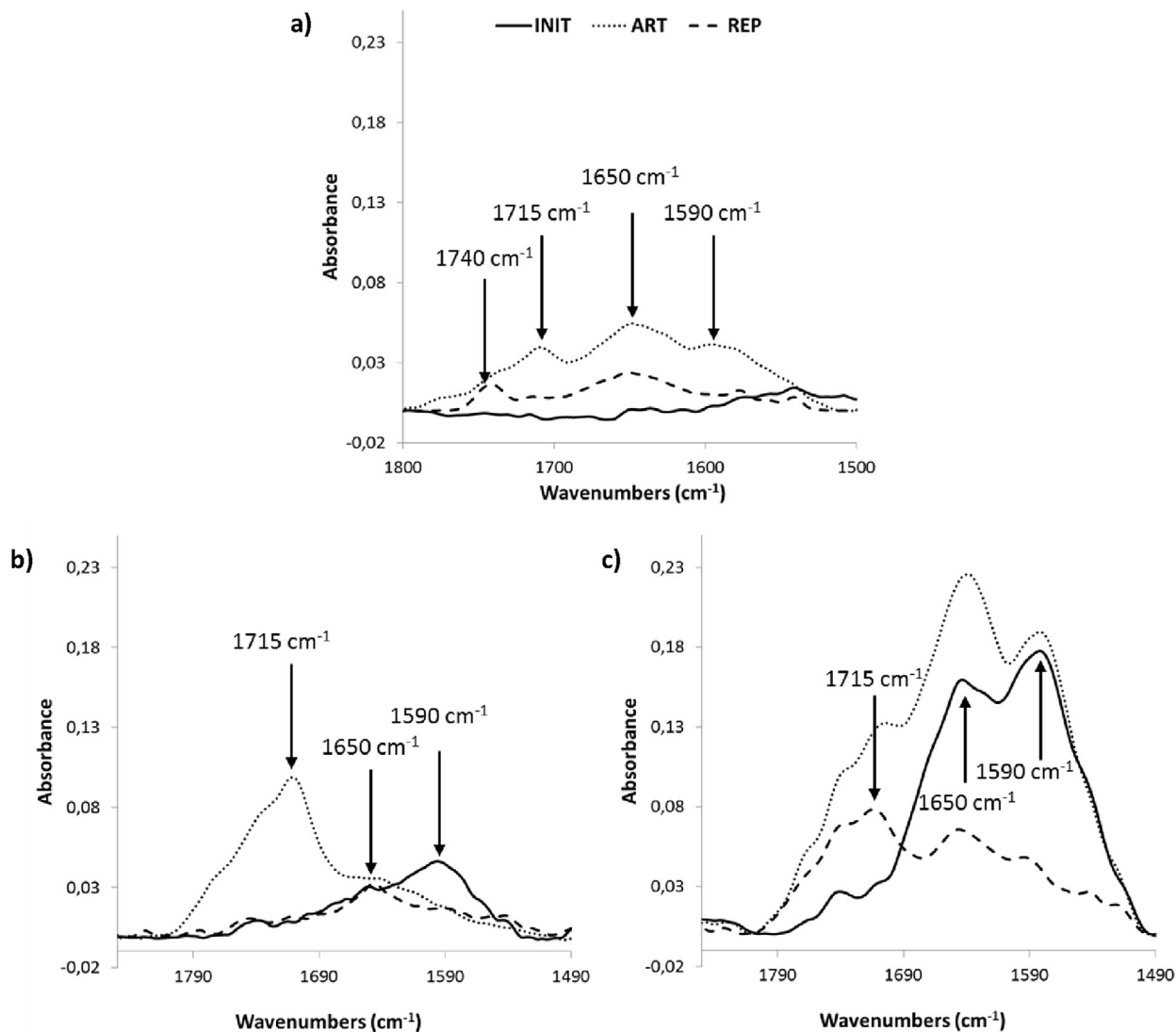


Fig. 9. Infrared spectrum in the carbonyl and vinyl range [1800–1500 cm^{-1}] of PP (a), PP/WF10 (b) and PP/WF30 (c) at every stage (INIT, ART and REP).

the ART stage, it can be observed that chain lengths are lower when the carbonyl intensities are the higher for every material (at the ART stage). So, the formation of carbonyl groups especially acid carboxylic ones is correlated with the chain scission mechanism of PP. In the PP/WF composites, the lignin degradation also leads to higher carbonyl intensity.

While comparing the three materials, trends are similar: the weathering induces the highest carbonyl absorbance and the strongest chain scission. The reprocessing of PP and PP/WF10 shows very low carbonyl indexes which are close to the initial values. Indeed, the carbonyl groups are mixed and diluted into the non-degraded matrix. Concerning PP/WF30, the REP stage shows an intermediate peak intensity value because of the protruded wood at the surface of the sample.

A scheme is proposed to understand the physical mechanisms observed in this study (Fig. 11). Degraded chains are drawn in blue while non-degraded chains are in red. At the initial state, the semi-crystalline PP is composed of non-degraded chains in crystalline and amorphous phases. At the weathering state (ART), the photo-oxidation induces a chain scission. It is well-known that this phenomenon is prevalent in amorphous phases because of the higher oxygen permeability [49]. The shorter chains tend to crystallize

thanks to their mobility and their ease to rearrange. Results from tensile elongation, impact tests, $T\alpha$ measurements by DMTA tests, crystallinity and viscosity measurements correlate well with the proposed mechanism. During the reprocessing by injection molding (REP), the molten state allow the degraded chains (mainly from the sample skin) and the non-degraded ones (mainly from the sample core) to be mixed together leading to a homogenized material as seen with the SEC results. During the cooling step, the degraded chains crystallize first and the amorphous phases are mainly composed of non-degraded chains. This explains the “regeneration” trend observed with tensile and impact tests and $T\alpha$ measurements as the amorphous phases are responsible of the measured properties. DMTA has also revealed for neat PP that the crystalline phases were composed of degraded chains with a significant shift of $T\alpha_c$ (Fig. 5a).

4. Conclusion

The aim of this work was to assess the influence of artificial UV weathering on the potential of reprocessing of spruce wood flour reinforced PP composites (grinding-injection molding cycles) with 10% w/w and 30% w/w of wood content. Numerous experiments

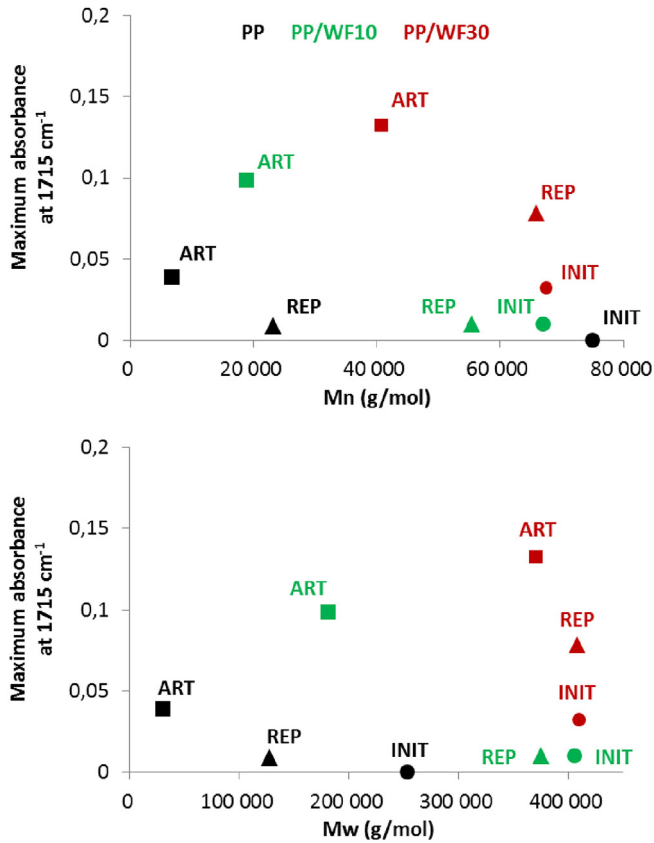


Fig. 10. Carbonyl absorbance at 1715 cm^{-1} as a function of \overline{M}_n and \overline{M}_w for PP (in black), PP/WF10 (in green) and PP/WF30 (in red) at every stage (● INIT, ■ ART and ▲ REP). (For interpretation of the references to color in this figure legend, the reader is referred to the web version of this article.)

were carried out at the initial (INIT), aged (ART) and reprocessed (REP) stages.

The visual observation of the surfaces after weathering has shown no significant variation for the neat PP and strong bleaching and micro cracking phenomena with wood protrusion at the surface for PP/WF composites. After reprocessing, the neat PP remains similar while the PP/WF composites display the disappearance of the bleaching effect and a darker brown color.

The static mechanical properties measured by tensile and impact tests have highlighted a “regeneration” phenomenon. Despite the mechanical degradation due to chain scission during photo-oxidation occurring at the ART step, the reprocessing step (REP) induces a recovering of their initial properties. Moreover, dynamic mechanical spectrometry carried out by DMTA has presented the same “regeneration” trend regarding the glass transition temperature (T_g) with a shift of $T_{g,c}$ peak after reprocessing. These relaxation temperatures were more difficult to detect for the PP/WF composites because of the wood particles restraining the PP macromolecular chain mobility. DSC, rheological and SEC tests have revealed a chain scission due to UV weathering. In particular, DSC and rheological tests have shown that the reprocessing step does not promote this chain scission furthermore. SEC results disclosed that the reprocessing step consists mainly in mixing degraded chains and non-degraded ones, leading to an intermediate average chain length. Otherwise, results suggest the better stability with higher wood content, probably due to lignin which could protect the composites from photodegradation due to its functions of stabilization and anti-oxidation or the opacification of the material limiting the UV light scattering into the polymer.

Infrared spectroscopy analyzes led us to conclude that the photo-degradation did occur for the wood flour and the PP matrix leading to carbonyl groups. The reprocessing step induces the mixing and the dilution of the degraded chains into the material and the injection of smooth samples with a low wood content at

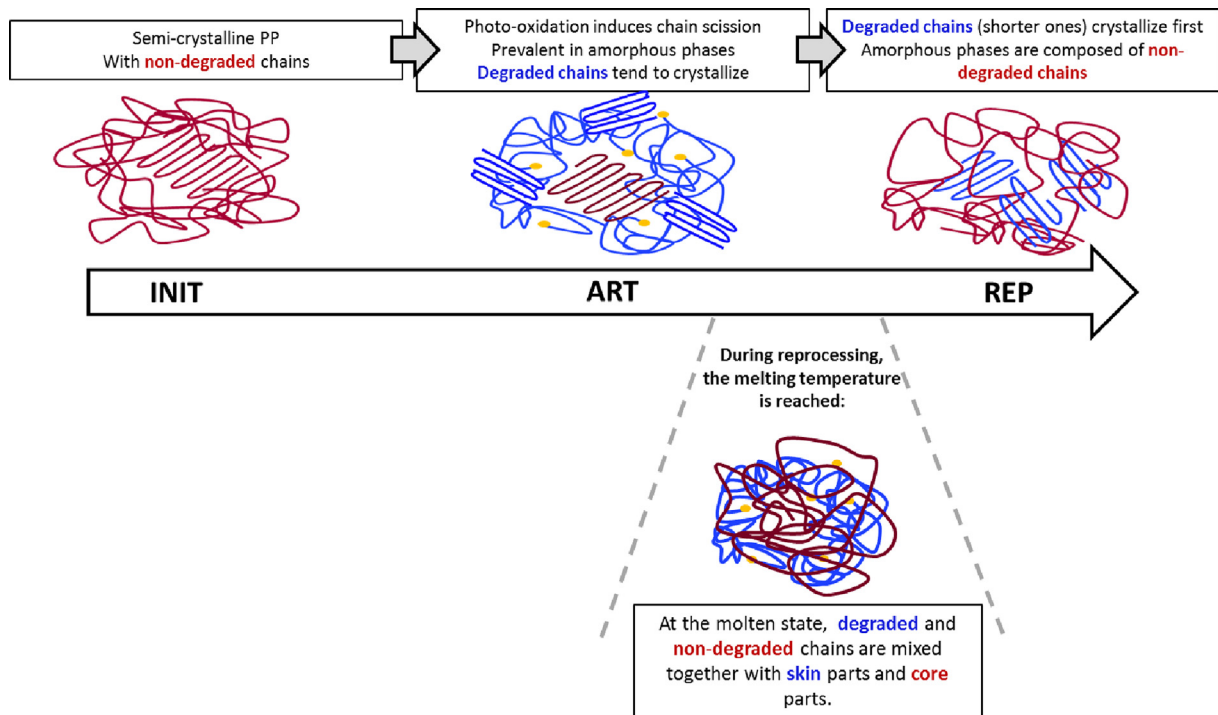


Fig. 11. Scheme of the microstructure evolution after weathering (ART) and reprocessing stages (REP).

the surface. Moreover, the formation of acid carboxylic groups was well correlated with the PP chain scission mechanism.

Acknowledgments

Authors are embedded to ADEME French Organization for the financial support (convention n° 1101C0066, acronym ENOLIBIO "END Of Life of BIOcomposites"), and would like to thank Mr. Jean-Marie Taulemesse for his assistance with scanning electron microscopy. The PIMM would like to thank the CARNOT-ARTS Institute for funding.

References

- [1] J.E. Winandy, N.M. Stark, C.M. Clemons, Considerations in recycling of wood-plastic composites, in: 5th Global Wood and Natural Fiber Composites Symposium, April 27–28, 2004 in Kassel, Germany.
- [2] J.A. Youngquist, G.E. Myers, J.M. Muehl, A.M. Krzysik, C.M. Clemons, Composites from Recycled Wood and Plastics, Final Report for U.S. Environmental Protection Agency, Project #IAGDW-12934608-2, USDA, Forest Service, Forest Products Laboratory, Madison WI, 1993.
- [3] K.B. Adhikary, S. Pang, M.P. Staiger, Dimensional stability and mechanical behaviour of wood-plastic composites based on recycled and virgin high-density polyethylene (HDPE), *Compos. Part B Eng.* 39 (2008) 807–815, <http://dx.doi.org/10.1016/j.compositesb.2007.10.005>.
- [4] L. Soccalingame, A. Bourmaud, D. Perrin, J.-C. Bénézet, A. Bergeret, Reprocessing of wood flour reinforced polypropylene composites: impact of particle size and coupling agent on composite and particle properties, *Polym. Degrad. Stab.* 113 (2015) 72–85, <http://dx.doi.org/10.1016/j.polydegradstab.2015.01.020>.
- [5] G. Guerrica-Echevarria, J.I. Eguiazabal, J. Nazabal, Effects of processing conditions on the properties of unfilled and talc-filled polypropylene, *Polym. Degrad. Stab.* 53 (1996) 1–8, [http://dx.doi.org/10.1016/0141-3910\(96\)00018-3](http://dx.doi.org/10.1016/0141-3910(96)00018-3).
- [6] J.J. Balatincez, M.M. Sain, The influence of recycling of wood fiber plastic composites, *Macromol. Symp.* 135 (1998) 167–173, <http://dx.doi.org/10.1002/masy.19981350119>.
- [7] S.V. Canevarolo, Chain scission distribution function for polypropylene degradation during multiple extrusions, *Polym. Degrad. Stab.* 70 (2000) 71–76, [http://dx.doi.org/10.1016/S0141-3910\(00\)00090-2](http://dx.doi.org/10.1016/S0141-3910(00)00090-2).
- [8] Q. Xiang, M. Xanthos, S. Mitra, S.H. Patel, J. Guo, Effects of melt processing on volatile emissions and structural/rheological changes of unstabilized polypropylene, *Polym. Degrad. Stab.* 77 (2002) 93–102, [http://dx.doi.org/10.1016/S0141-3910\(02\)00083-6](http://dx.doi.org/10.1016/S0141-3910(02)00083-6).
- [9] M.H. Martins, M.A. De Paoli, Polypropylene compounding with post-consumer material: II. Processing, *Polym. Degrad. Stab.* 78 (2002) 491–495, [http://dx.doi.org/10.1016/S0141-3910\(02\)00195-7](http://dx.doi.org/10.1016/S0141-3910(02)00195-7).
- [10] H.M. da Costa, V.D. Ramos, Marisa C.G. Rocha, Rheological properties of polypropylene during multiple extrusion, *Polym. Test.* 24 (2005) 86–93, <http://dx.doi.org/10.1016/j.polymertesting.2004.06.006>.
- [11] C. Meran, O. Ozturk, M. Yuksel, Examination of the possibility of recycling and utilizing recycled polyethylene and polypropylene, *Mater. Des.* 29 (2008) 701–705, <http://dx.doi.org/10.1016/j.matdes.2007.02.007>.
- [12] S. Kazemi-Najafi, M. Mostafazadeh- Marznaaki, M. Chaharmahali, M. Tajvidi, Effect of thermo-mechanical degradation of polypropylene on mechanical properties of wood-polypropylene composites, *J. Compos. Mater.* 43 (2009) 2543–2554, <http://dx.doi.org/10.1177/0021998309345349>.
- [13] N. Bahlouli, D. Pessey, C. Raveyre, J. Guillet, S. Ahzi, A. Dahoun, J.M. Hiver, Recycling effects on the rheological and thermomechanical properties of polypropylene-based composites, *Mater. Des.* 33 (2012) 451–458, <http://dx.doi.org/10.1016/j.matdes.2011.04.049>.
- [14] C. Sadrmohaghegh, G. Scott, Effect of reprocessing on polymers: part II—polypropylene, *Polym. Degrad. Stab.* 3 (1981) 333–340, [http://dx.doi.org/10.1016/0141-3910\(81\)90039-2](http://dx.doi.org/10.1016/0141-3910(81)90039-2).
- [15] S. Migneault, A. Koubaa, F. Erchiqui, A. Chaala, K. Englund, M.P. Wolcott, Effects of processing method and fiber size on the structure and properties of wood-plastic composites, *Compos. Part A Appl. Sci. Manuf.* 40 (2009) 80–85, <http://dx.doi.org/10.1016/j.compositesa.2008.10.004>.
- [16] A. Bourmaud, C. Baley, Investigations on the recycling of hemp and sisal fiber reinforced polypropylene composites, *Polym. Degrad. Stab.* 92 (2007) 1034–1045, <http://dx.doi.org/10.1016/j.polydegradstab.2007.02.018>.
- [17] A. Bourmaud, A. Le Duigou, C. Baley, What is the technical and environmental interest in reusing a recycled polypropylene-hemp fibre composite? *Polym. Degrad. Stab.* 96 (2011) 1732–1739, <http://dx.doi.org/10.1016/j.polydegradstab.2011.08.003>.
- [18] L. Augier, G. Sperone, C. Vaca-Garcia, M.-E. Borredon, Influence of the wood fibre filler on the internal recycling of poly(vinyl chloride)-based composites, *Polym. Degrad. Stab.* 92 (2007) 1169–1176, <http://dx.doi.org/10.1016/j.polydegradstab.2007.04.010>.
- [19] Z.N. Azwa, B.F. Yousif, A.C. Manalo, W. Karunasena, A review on the degradability of polymeric composites based on natural fibres, *Mater. Des.* 47 (2013) 424–442, <http://dx.doi.org/10.1016/j.matdes.2012.11.025>.
- [20] D.E. Pendleton, T.A. Hoffard, T. Adcock, B. Woodward, M.P. Wolcott, Durability of an extruded HDPE/wood composite, *For. Prod. J.* 52 (2002) 21–27.
- [21] M. Mankowski, J.J. Morrell, Patterns of fungal attack in wood-plastic composites following exposure in a soil block test, *Wood Fiber Sci.* 32 (2000) 340–345.
- [22] M.D.H. Beg, K.L. Pickering, Accelerated weathering of unbleached and bleached kraft wood fibre reinforced polypropylene composites, *Polym. Degrad. Stab.* 93 (2008) 1939–1946, <http://dx.doi.org/10.1016/j.polydegradstab.2008.06.012>.
- [23] W. Wang, M. Sain, P.A. Cooper, Hygrothermal weathering of rice hull/HDPE composites under extreme climatic conditions, *Polym. Degrad. Stab.* 90 (2005) 540–545, <http://dx.doi.org/10.1016/j.polydegradstab.2005.03.014>.
- [24] L.M. Matuana, S. Jin, N.M. Stark, Ultraviolet weathering of HDPE/wood-flour composites coextruded with a clear HDPE cap layer, *Polym. Degrad. Stab.* 96 (2011) 97–106, <http://dx.doi.org/10.1016/j.polydegradstab.2010.10.003>.
- [25] Y. Peng, R. Liu, J. Cao, Y. Chen, Effects of UV weathering on surface properties of polypropylene composites reinforced with wood flour, lignin, and cellulose, *Appl. Surf. Sci.* 317 (2014) 385–392, <http://dx.doi.org/10.1016/j.apsusc.2014.08.140>.
- [26] Y. Peng, R. Liu, J. Cao, Characterization of surface chemistry and crystallization behavior of polypropylene composites reinforced with wood flour, cellulose, and lignin during accelerated weathering, *Appl. Surf. Sci.* 332 (2015) 253–259, <http://dx.doi.org/10.1016/j.apsusc.2015.01.147>.
- [27] S.K. Najafi, Use of recycled plastics in wood plastic composites – a review, *Waste Manag.* 33 (2013) 1898–1905, <http://dx.doi.org/10.1016/j.wasman.2013.05.017>.
- [28] A. Jansson, K. Möller, T. Gevert, Degradation of post-consumer polypropylene materials exposed to simulated recycling—mechanical properties, *Polym. Degrad. Stab.* 82 (2003) 37–46, [http://dx.doi.org/10.1016/S0141-3910\(03\)00160-5](http://dx.doi.org/10.1016/S0141-3910(03)00160-5).
- [29] S. Luzuriaga, J. Kovářová, I. Fortelný, Degradation of pre-aged polymers exposed to simulated recycling: properties and thermal stability, *Polym. Degrad. Stab.* 91 (2006) 1226–1232, <http://dx.doi.org/10.1016/j.polydegradstab.2005.09.004>.
- [30] F. Vilaplana, S. Karlsson, Quality concepts for the improved use of recycled polymeric materials: a review, *Macromol. Mater. Eng.* 293 (2008) 274–297, <http://dx.doi.org/10.1002/mame.200700393>.
- [31] ATLAS Material Testing Solutions, "Benchmark Climates" (n.d.), Retrieved June 17th 2014 online, from internet website: <http://atlas-mts.com/services/natural-weathering-testing-services/static-weathering/benchmark-climates/>.
- [32] L.H. Sperling, Introduction to Physical Polymer Science, fourth ed., John Wiley & Sons Inc, 2006, ISBN 9780471757115, p. 244.
- [33] J. Laffargue, Etude et modélisation des instabilités du procédé de soufflage de gaine, PhD thesis in Material Science and Engineering, Ecole des Mines de Paris, Paris, 2003, p. 168.
- [34] S. Havriliak, S. Negami, A complex plane representation of dielectric and mechanical relaxation processes in some polymers, *Polymer* 8 (1967) 161–210, [http://dx.doi.org/10.1016/0032-3861\(67\)90021-3](http://dx.doi.org/10.1016/0032-3861(67)90021-3).
- [35] L.M. Matuana, N.M. Stark, Surface chemistry changes of weathered HDPE/wood flour composites studied by XPS and FTIR spectroscopy, *Polym. Degrad. Stab.* 86 (2004) 1–9, <http://dx.doi.org/10.1016/j.polydegradstab.2003.11.002>.
- [36] K.K. Pandey, T. Vuorinen, Comparative study of photodegradation of wood by a UV laser and a xenon light source, *Polym. Degrad. Stab.* 93 (2008) 2138–2146, <http://dx.doi.org/10.1016/j.polydegradstab.2008.08.013>.
- [37] K. Chaochanchaikul, K. Jayaraman, V. Rosarpitak, N. Sombatsompop, Influence of lignin content on photodegradation in wood/HDPE composites under UV weathering, *BioResources* 7 (2012) 38–55, 18p.
- [38] B. Fayolle, E. Richaud, J. Verdu, F. Farcas, Embrittlement of polypropylene fibre during thermal oxidation, *J. Mater. Sci.* 43 (2008) 1026–1032, <http://dx.doi.org/10.1007/s10853-007-2242-1>.
- [39] A.A. Morandim-Giannetti, J.A.M. Agnelli, B.Z. Lanças, R. Magnabosco, S.A. Casarin, S.H.P. Bettini, Lignin as additive in polypropylene/coir composites: thermal, mechanical and morphological properties, *Carbohydr. Polym.* 87 (2012) 2563–2568, <http://dx.doi.org/10.1016/j.carbpol.2011.11.041>.
- [40] C. Pouteau, P. Dole, B. Cathala, L. Averous, N. Boquillon, Antioxidant properties of lignin in polypropylene, *Polym. Degrad. Stab.* 81 (2003) 9–18, [http://dx.doi.org/10.1016/S0141-3910\(03\)00057-0](http://dx.doi.org/10.1016/S0141-3910(03)00057-0).
- [41] S. Farzaneh, A. Tcharhktchi, Viscoelastic properties of polypropylene reinforced with mica in and transition zones, *Int. J. Polym. Sci.* (2011), <http://dx.doi.org/10.1155/2011/427095>.
- [42] L.E. Nielsen, R.F. Landel, Particle-filled Polymers, Mechanical Properties of Polymers and Composites, second ed., Marcel Dekker, New York, NY, USA, 1994.
- [43] A. Etaati, S. Pather, Z. Fang, H. Wang, The study of fibre/matrix bond strength in short hemp polypropylene composites from dynamic mechanical analysis, *Compos. Part B Eng.* 62 (2014) 19–28, <http://dx.doi.org/10.1016/j.compositesb.2014.02.011>.
- [44] V. Verney, Rheology, oxidation and polymer aging, *Rhéologie* 13 (2008).
- [45] H. Askanian, Etude de la durabilité de matériaux respectueux de l'environnement/biocomposites, PhD thesis in Chemistry-Physics, Université Blaise Pascal, Clermont-Ferrand, 2011, p. 164.
- [46] S. Butylina, M. Hyvärinen, T. Kärki, A study of surface changes of

- wood–polypropylene composites as the result of exterior weathering, *Polym. Degrad. Stab.* 97 (2012) 337–345, <http://dx.doi.org/10.1016/j.polymdegradstab.2011.12.014>.
- [47] J.S. Fabiyi, A.G. McDonald, M.P. Wolcott, P.R. Griffiths, Wood plastic composites weathering: visual appearance and chemical changes, *Polym. Degrad. Stab.* 93 (2008) 1405–1414, <http://dx.doi.org/10.1016/j.polymdegradstab.2008.05.024>.
- [48] A. François-Heude, E. Richaud, E. Desnoux, X. Colin, A general kinetic model for the photothermal oxidation of polypropylene, *J. Photochem. Photobiol. A Chem.* 296 (2015) 48–65, <http://dx.doi.org/10.1016/j.jphotochem.2014.08.015>.
- [49] S. Suzuki, Y. Nakamura, A.T.M.K. Hasan, B. Liu, M. Terano, H. Nakatani, Dependence of tacticity distribution in thermal oxidative degradation of polypropylene, *Polym. Bull.* 54 (2005) 311–319, <http://dx.doi.org/10.1007/s00289-005-0389-y>.